Drainage Effects in a Dilatant Carbonate Silty Sand

Farnoud Farzaneganpour[1#], *Fraser* Bransby[1] and *Conleth* O'Loughlin[1]

[1]*Centre for Offshore Foundation Systems, Oceans Graduate School, The University of Western Australia, Perth, WA, Australia*
[#]*Corresponding author: farnoud.farzaneganpour@research.uwa.edu.au*

ABSTRACT

This paper presents and discusses results from a series of cone, vane and footing tests in a carbonate silty sand, conducted in a geotechnical centrifuge, that investigate how drainage effects scale with the diameter of the device/foundation. The tests involved different penetration and rotational velocities to quantify how velocity influences the drainage response, and in turn, the magnitude of the deduced soil strength. Cone and foundation resistance, and the shear stress measured in the vane tests, were seen to increase with increasing penetration/rotational velocity, consistent with a dilatant shearing response. The collective dataset is interpreted within the 'drainage backbone curve' framework, with an attempt made to understand how drainage path length varies for the different devices and is affected by stress level.

Keywords: drainage, carbonate silty sand, dilatant, footing, cone penetrometer, vane shear

1. Introduction

1.1. Background

In offshore geotechnical design, a crucial requirement is the reliable prediction of soil strength at various stages in the lifespan of an offshore foundation. The shear strength of soil supporting such a foundation can undergo changes due to factors like drainage/consolidation, strain softening (partial or full remoulding), and viscous rate effects. The significance of some of these effects varies depending on the soil type; for example, strain rate effects may be negligible in coarse-grained soils.

In situ penetrometer tests, whether using a cone or full flow penetrometer, offer the advantage of modelling the aforementioned effects. However, conventional cone penetrometer tests typically involve penetration at the industry standard velocity of 2 cm/s (for a 10 cm^2 cone). In fine-grained soils the measured penetration resistance is often used to establish the undrained shear strength under the assumption that penetrating at 2 cm/s will generate undrained conditions. In contrast, for coarse grained soils, the penetration resistance is often used to estimate the relative density of the soil, with the assumption that penetrating at 2 cm/s generates drained conditions. However, for intermediate soils the reality is quite often somewhere in-between, i.e., neither fully drained nor fully undrained.

There have been several experimental studies over the past couple of decades that have quantified the effect of penetration rate – and hence drainage conditions – on the response of clays and silts that exhibit a contractile response during shearing (e.g. Finnie and Randolph 1994; House et al. 2001; Randolph and Hope 2004; Mahmoodzadeh and Randolph 2014; Chow et al. 2020). In contrast there have been very few equivalent studies in soils that dilate during shearing (Wroth et al. 2022).

These studies account for changing drainage conditions through a dimensionless velocity:

$$V = \frac{vD}{c_v} \; or \; V' = \frac{vD}{c_h} \tag{1}$$

where v is the penetration velocity, D is the diameter (and assumed to be proportional to the drainage path length) and c_v or c_h are the vertical or horizontal coefficients of consolidation, respectively.

The above studies quantify the variation of penetrometer or footing resistance, q, with dimensionless velocity, V, (or V'), with different threshold values of dimensionless velocity proposed to identify the transition to drained and undrained resistance. The change in resistance with dimensionless velocity can be approximated using a 'back-bone curve' of the form (Lee and Randolph 2011):

$$\frac{q}{q_u} = 1 + \frac{\frac{q_d}{q_u} - 1}{(1 + (V/V_{50})^d)} \tag{2}$$

where q_u is the undrained resistance, q_d is the drained resistance, V_{50} is the dimensionless velocity V associated with 50% consolidation, and d is an exponent that controls the steepness of the backbone curve (and hence how abruptly resistance changes with increasing dimensionless velocity).

Different studies have recommended different values of V_{50} for different boundary value problems and soil types (Finnie and Randolph 1994; Chow et al. 2020; Wroth et al. 2022). It remains unclear whether these disparities are to do with differences in drainage length scales for different devices (compared to the device diameter, for example), or because of errors in quantifying c_v or c_h.

This study explores whether drainage condition scales with the dimension of the foundation or the in situ strength measurement device by performing tests on different devices (at different embedments) in a single soil sample. The tests were conducted in a geotechnical

centrifuge using a reconstituted carbonate silty sand, recovered from the near-surface seabed on the North West Shelf of Australia in approximately 100 m water depth.

2. Experimental methods

2.1. Overview

The experimental programme was carried out in the small beam geotechnical centrifuge (Randolph et al. 1991) located at the National Geotechnical Centrifuge Facility (NGCF) in the University of Western Australia (UWA). The programme was conducted at a testing acceleration of 30g and included cone penetration tests (CPTs), vane shear tests and circular foundation tests. Drainage conditions were varied in the tests by penetrating the cone penetrometer and footing at different velocities, and by rotating the vane at different rotational velocities. Details of the equipment are as follows:

- a 10 mm diameter piezocone penetrometer (with the separately measurement of tip resistance, 'u_2' pore pressure and sleeve friction),
- a 40 mm diameter footing (with a pore pressure transducer located at the centre of the foundation base), and
- a vane shear device with two different blade diameters: 19 mm and 29 mm (both with a blade height of 29 mm).

One sample of carbonate silty sand was prepared in a sample container (or 'strongbox') with plan dimensions of 1300 by 390 mm and a depth of 325 mm. A schematic view of the individual tests is shown in Fig.1.

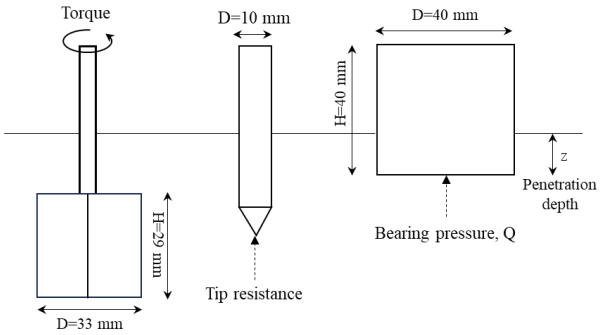

Figure 1. Schematic view of the vane shear, piezocone and circular foundation.

2.2. Sample preparation

The sample was prepared using a carbonate silty sand with a 44% fines content, median grain size, d_{50} = 0.085 mm and carbonate content of 92% (O'Beirne et al. 2020). Oedometer tests on this soil indicated that for the tests described here, the representative vertical coefficient of consolidation, c_v = 100 m^2/year, while the dissipation stage of a piezocone test (conducted in a different sample) indicated a representative horizontal coefficient of consolidation, c_h = 210 m^2/year (O'Beirne et al. 2020).

The carbonate silty sand was mixed by hand to a moisture content of 40% and placed (by hand) in three layers into the strongbox, each compacted with 15 blows of a 2 kg weight from a height of approximately 200 mm. The sample was then submerged with tap water with free water height of 50 to 60 mm to create a saturated condition and then consolidated in the centrifuge at 150g (after a gradual ramp-up with pauses at 5g, 25g and 60g to prevent segregation). Settlement of the sample surface during self-weight consolidation was monitored with a linear displacement transducer. These measurements indicated that consolidation was essentially complete after approximately 3 hours. Two spin up/down cycles to 150g were then performed in an attempt to 'shake-down' the sample to an equilibrium density state. The sample (which was then 72 mm deep) was then spun at the testing acceleration of 30g such that during testing the over consolidation ratio, OCR = 5.

2.3. Cone penetrometer and footing tests

The piezocone penetrometer and footing tests were conducted using an electro-mechanical actuator at vertical penetration rates in the range, v = 0.001 mm/s to v = 170 mm/s. The model scale piezocone has a diameter, D = 10 mm and a sleeve length of 37.5 mm.

2.4. Vane shear test

The vane shear tests were carried out using a rotary actuator capable of rotating at a maximum speed of 90 deg/s (following installation at a vertical rate up to 4 mm/s), providing a torque load of up to 25 Nm, with a torque load cell capacity limited to 5.5 Nm.

The testing programme included four vane shear tests conducted at rates of 0.36, 3.6, 36, and 90 deg/s for each of the two vane diameters. High-speed data acquisition at 20 kHz was employed for the two fastest tests. The tests conducted at rates of 3.6, 36, and 90 deg/s were installed vertically at 4 mm/s, while the slowest test had a penetration rate of 0.1 mm/s. The target depth (for the bottom of the vane) for all tests was 50 mm, so that the middle of the vane was mid-depth in the soil. A waiting period of 120 seconds was adopted for the slowest test, whereas rotation commenced immediately upon reaching the target depth for the other tests.

3. Results

3.1. Cone penetration

Cone tip resistance is plotted against normalised cone tip depth (z/D, where z is the depth and D is the cone diameter) in Fig. 2 for all the cone penetration tests. The tests cover velocities ranging from v = 0.0015 mm/s (light blue) to v = 170 mm/s (black). Cone tip resistance, q_c, is larger at faster penetration velocities, indicating a dilating response of the soil. Additionally, cone resistance increases with depth, reflecting both higher stress levels and mechanism changes from unconstrained near the surface to cavity expansion when deeper (e.g. Puech and Foray 2002). However, in tests conducted under drained and partially drained conditions, the base boundary effect is encountered after penetrating by 6 cone diameters. This is attributed to the localised shear-induced zone in undrained conditions, while in drained

conditions, the shear-induced zone is larger, resulting in earlier 'sensing' of the base boundary.

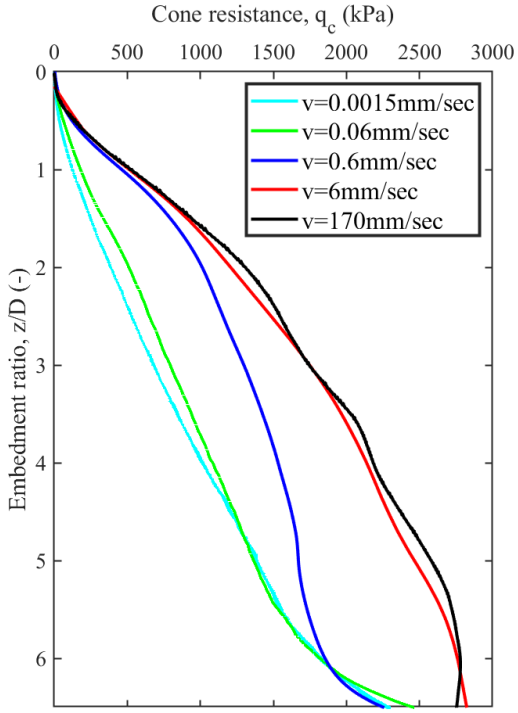

Figure 2. Cone tip resistance for CPTs with different penetration velocities.

The variation in cone tip resistance with penetration velocity is examined further in Figure 3, which shows the ratio of cone tip resistance, q_c, to the drained cone tip resistance, $q_{c,d}$ (taken from the slowest cone test at v = 0.001 mm/sec), against dimensionless velocity, V' (see Eq. 1). V' (rather than V) is adopted in Figure 3 as drainage is expected to be mostly radial, such that the use of c_h rather than c_v in preferred (Lehane et al. 2009; Mahmoodzadeh and Randolph 2014; Colreavy et al. 2016a, 2016b).

As the penetration depth increases, the ratio of undrained to drained cone resistance decreases from 4.1 for z/D = 1 to 1.5 for z/D = 6. This change cannot only be attributed to shallow embedment effects, as the equivalent ratio was 12 at z/D = 4 from piezocone tests on the same soil (Wroth et al. 2022). The Wroth et al. (2022) piezocone tests were conducted at a much lower stress level and higher OCR, resulting in greater dilation, explaining the difference in the ratio of drained to undrained cone resistance.

Figure 3 also shows backbone curves obtained using the following modification of equation 2 (Wroth et al., 2022):

$$\frac{q}{q_d} = a - \frac{a-1}{(1+(V'/V'_{50})^d} \quad (3)$$

where a is the ratio of undrained to drained cone resistance, q_u/q_d, established from q_c measurements in the fastest and slowest tests. Eq. 3 is seen to provide good agreement with the measurements for all embedment depths using the d and V'_{50} values summarised in Table 1.

Values of a (i.e., the ratio of undrained to drained cone resistance) are broadly consistent with values of undrained soil strength calculated from critical state principles, but with allowance made for a cavitation-induced limit on negative excess pore pressure.

Table 1. Equation 3 parameters for CPTs at different embedment ratios

z/D	a	d	V'_{50}
1	4.1	1.5	0.3
2	3.0	1	0.5
3	2.5	1	0.7
4	2.2	1.5	1
5	2.0	2	2
6	1.8	3	4

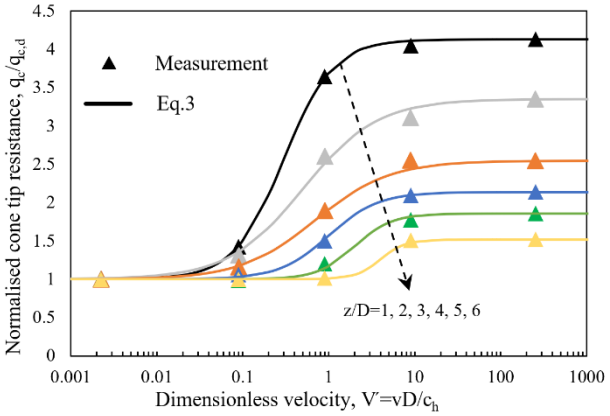

Figure 3. Backbone curves derived from cone penetration at different embedment ratios.

As can be seen in Fig. 3, V'_{50} increases with penetration depth (so you have to move the cone faster to achieve partially drained conditions) and is expected to be asymptoting to a fixed value for large depths. In addition, it can be concluded that at all depths, undrained conditions are achieved with $V' \geq 10$ and there is no further increase with increasing velocity. It should be noted that drained conditions are achieved at different velocities depending on penetration depth, changing by two orders of magnitude between z/D = 1 (at V' ≈ 1) and z/D = 6 (at about V' ≈ 0.01)

3.2. Circular footing penetration

Soil bearing resistance is plotted against footing base depth in Fig. 4 for the circular footing tests at rates from v = 0.001 to v = 70 mm/s. The bearing resistance increases with the penetration velocity, consistent with expectations for dilatant soil.

The cone penetration data indicate that conditions were undrained when $V' \geq 10$ (equivalent to a penetration velocity of 6 mm/s for a 10 mm cone). Consequently, it is inferred that the footing penetration with v = 70 mm/s should be undrained, given that the footing diameter is four times that of the cone diameter. Similarly, the footing test with a penetration velocity of 1.5 mm/s should also be undrained, with V = 10, assuming the drainage path length of the footing, L, is equal to the footing diameter as suggested by Finnie & Randolph (1994) (i.e., L = D). However, pore pressure measurements at the base of the footing (shown in Fig. 5) suggest that none of the tests measured pore pressures

equal to the applied total stress (which would be expected for fully undrained conditions at the footing centre). Even in the fastest test, the ratio of pore pressure to bearing pressure is approximately 70%.

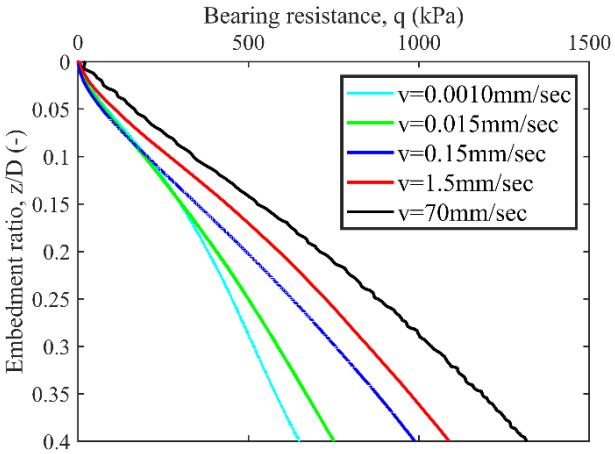

Figure 4. Depth profile of bearing resistances from circular footing tests at different penetration velocities.

While this suggests that a fully undrained condition has not been achieved, it should be noted that since the pore pressure transducer is located at the footing base, individual pore pressures at that point are likely to dissipate faster than the overall system due to its proximity to the free-surface (and being on a potential preferential drainage path on the footing interface). Hence, the pore pressure sensor measurement at the bottom of the footing is unlikely to directly represent the overall drainage condition (apart from fully drained or fully undrained conditions). Therefore, the fastest test is unlikely to be fully undrained but is likely to be more than 70% from drained to undrained.

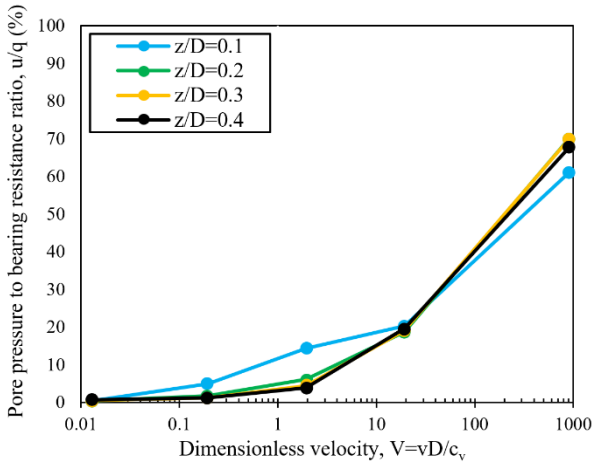

Figure 5. Ratio of pore pressure to bearing resistance, u/q against dimensionless velocity

Given that fully undrained conditions were not achieved in any of the footing tests, backbone curves to fit the data using Eq. 3 with the details shown in Table 2 are plotted in Fig. 6.

The V_{50} values to fit the data reduce with increasing embedment, which contrasts with the reduction with embedment seen for the CPTs. Not achieving fully undrained condition at a similar velocity compared to cone penetration on a footing quadruple the size of the cone suggests that the drainage path length is not always proportional to diameter.

Table 2. Equation 3 parameters for footing at different embedment ratio

z/D	a	d	V_{50}
0.1	1.9	0.8	40
0.2	2.07	0.5	20
0.3	2.2	0.5	12
0.4	2.2	0.5	10

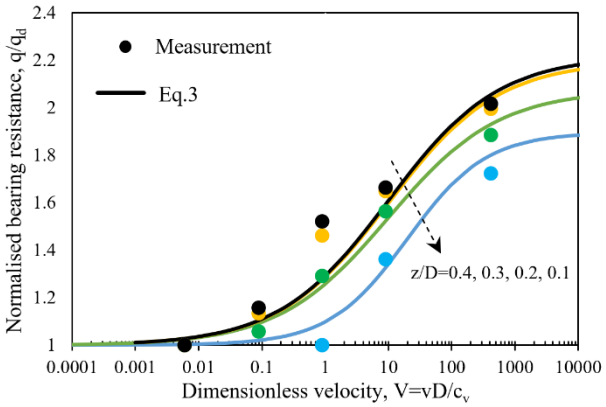

Figure 6. Normalised bearing resistance at different embedment depths against dimensionless velocity (assuming drainage path length equals the footing diameter; L = D)

3.3. Vane shear test

Vane shear tests were included in the testing programme to further investigate changes in strength and the relationship between drainage path length and diameter. These tests utilised two vanes with diameters of 19 mm and 33 mm, each with a height of 29 mm. Results from tests using the smaller vane are shown on Fig. 7. These results exhibit a peak strength at rotations of between 15 and 20 degrees, reducing to a steady state strength of about 10 kPa (for each rotation rate) after about 80 degrees rotation. The peak strength is seen to be dependent on rotation rate, with higher rotation rates corresponding with higher soil strengths. A limiting peak strength is apparent at 36 deg/sec, as the strength at this rotation rate and in two tests at 90 deg/sec gave the same peak strength. The jumps in the shear stress response in the 36 deg/sec test is due to an issue with the actuation control, which caused the rotational velocity to vary between 17 and 69 deg/s, but with an average value of 36 deg/sec.

Again, since no strain rate effect is expected in this soil type, the increase in strength is attributed to the generation of negative excess pore pressure and soil dilatancy potential during shearing in the faster tests, as also observed in the cone and footing tests. However, the invariance of residual strength (at large rotations) to rotation rate is unexpected, as despite the relatively high sensitivity of carbonate silty sand, variations in mobilised strength were anticipated due to differences in drainage conditions.

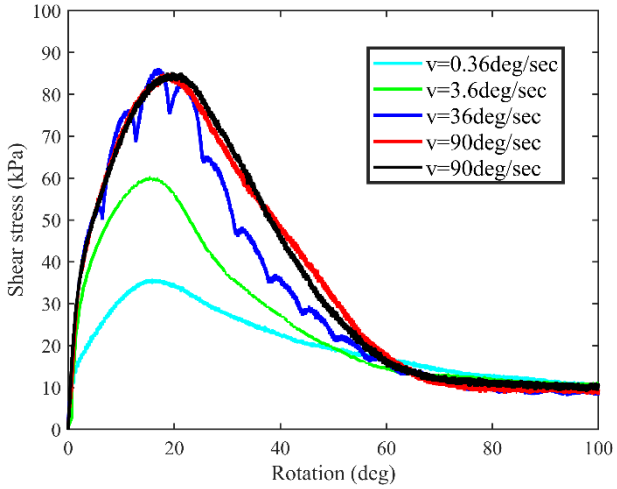

Figure 7. Soil response from vane shear tests at different rotational rates.

Fig. 8 plots the ratio of peak strengths, expressed as $\tau_p/\tau_{p,d}$, where the drained peak strength, $\tau_{p,d}$, was assumed to have been mobilised in the slowest test (at 0.36 deg/s). Eq. 3 was fitted to the data on Fig. 8 using the parameters listed in Table 3, with the assumption that undrained conditions developed in the fastest test (supported by observations made from Fig. 7 as discussed earlier). The match between the measurements and Eq. 3 on Fig. 8 is reasonable, given the lack of data at intermediate values of dimensionless velocity.

Table 3. Equation 3 parameters for vane shear at different embedment ratios

z/D	a	d	V'_{50}
1	1.55	1.5	5
1.7	2.4	1.5	1.5

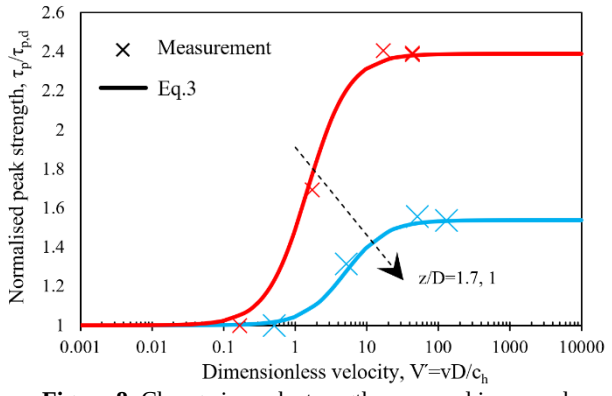

Figure 8. Change in peak strength measured in vane shear tests for different dimensionless velocities (assuming drainage path length is equal to the vane diameter)

Although the rotational velocity of both vanes was similar, the circumferential velocity for a given rotational velocity differs between the two vanes. Hence, while it is anticipated that two vanes at a given rotational velocity (e.g., 0.36 deg/sec) would have a similar drainage condition, the larger vane would experience a greater circumferential velocity. This difference could result in different drainage conditions and therefore breach the initial assumption that the slowest test in both vanes represents the drained condition. Whilst the different ratios of fully undrained to drained resistance may be attributed to this discrepancy in circumferential velocity, the consistent resistances observed in the five tests conducted at 36 and 90 deg/sec on both vanes make this assumption unlikely. Other factors, such as different cavity expansion due to vane insertion and during shearing could also contribute to the variation in the peak strength ratio.

4. Drainage path lengths

As observed in the previous sections, different V_{50} values were required to fit the observed drainage transition curves for the different devices, and for the different devices at different embedment depths (Table 1, Table 2 and Table 3). Another way of considering these differences is to consider that a single drainage transition curve with a normalised V_{50} = 1 may be used for all devices at all depths if an equivalent drainage length, αD can be selected for each particular device and embedment. The value of α can be selected simply as $\alpha = 1/V_{50,device}$ and the resulting relationship is plotted in Fig. 8 for the cone and footing.

Fig. 8 compares α for the three different devices at different embedment depths. Drainage length factor α reduces with embedment depth for the cone, whereas α increases with embedment depth for the footing. At an embedment, z = 16 mm, α is approximately 24 times lower than that of the cone, indicating differences in drainage path length between the cone and the footing. The trend in α for the footing is expected as deeper embedment would require a longer drainage path length, requiring a higher multiplier on the footing diameter, i.e., higher α. The reduction in α with depth for the cone is considered to reflect the change in failure mechanism as the cone becomes deeper.

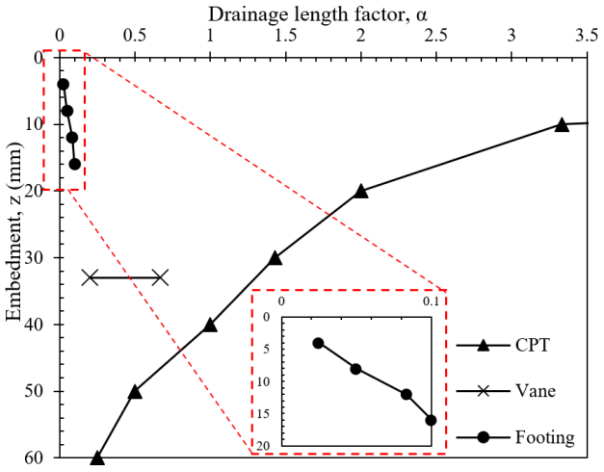

Figure 9. Values of the drainage length factor, α, for the cone, vane shear and footing

5. Conclusions

A series of vane shear, piezocone, and footing tests at varying rotational and penetration velocities were conducted in a beam centrifuge on a natural carbonate silty sample, representative of near surface offshore density states. The objective was to examine how seabed

resistance varies with changing soil drainage conditions. Backbone curves were derived for each device, all indicating dilatant behaviour of the soil, with the degree of dilatancy changing according to stress levels.

It was also noted that the drainage path length does not always scale in the same way with the diameter of the device so the drainage transition curve may require modification.

Acknowledgements

This work was supported by the Australia Research Council Discovery Programme (Grant No. DP200103468). The second author acknowledges the support of Fugro, provided via the Fugro Chair in Geotechnics at UWA.

References

Chow, S. H., C. D. O'Loughlin, Z. Zhou, D. J. White, and M. F. Randolph. 2020. "Penetrometer Testing in a Calcareous Silt to Explore Changes in Soil Strength." *Geotechnique* 70 (12): 1160–73. https://doi.org/https://doi.org/10.1680/jgeot.19.P.069.

Colreavy, C., C. D. O'Loughlin, and M. F. Randolph. 2016a. "Estimating Consolidation Parameters from Field Piezoball Tests." *Geotechnique* 66 (4): 333–43. https://doi.org/10.1680/jgeot.15.P.106.

Colreavy, C., C. D. O'Loughlin, and M. F. Randolph. 2016b. "Experience with a Dual Pore Pressure Element Piezoball." *International Journal of Physical Modelling in Geotechnics* 16 (3): 101–18. https://doi.org/10.1680/JPHMG.15.00011.

Finnie, I. M. S., and M.F. Randolph. 1994. "Punch-through and Liquefaction Induced Failure of Shallow Foundations on Calcareous Sediments." *Proceedings of International Conference on Behaviour of Offshore Structures, Boston*, 217–30.

House, A.R., J.R.M.S. Oliveira, and M.F. Randolph. 2001. "Evaluating the Coefficient of Consolidation Using Penetration Tests." *International Journal of Physical Modelling in Geotechnics* 1 (3): 17–26. https://doi.org/10.1680/ijpmg.2001.010302.

Lee, J., and M.F. Randolph. 2011. "Penetrometer-Based Assessment of Spudcan Penetration Resistance." *Journal of Geotechnical and Geoenvironmental Engineering* 137 (6): 587–96. https://doi.org/10.1061/(asce)gt.1943-5606.0000469.

Lehane, B. M., C. D. O'Loughlin, C. Gaudin, and M. F. Randolph. 2009. "Rate Effects on Penetrometer Resistance in Kaolin." *Geotechnique* 59 (1): 41–52. https://doi.org/10.1680/GEOT.2007.00072.

Mahmoodzadeh, H., and M. F. Randolph. 2014. "Penetrometer Testing: Effect of Partial Consolidation on Subsequent Dissipation Response." *Journal of Geotechnical and Geoenvironmental Engineering* 140 (6). https://doi.org/10.1061/(ASCE)GT.1943-5606.0001114.

O'Beirne, C., C. D. O'Loughlin, P. Watson, and D. J. White. 2020. "Centrifuge Modelling of Pipe Clamping Mattresses (PCMs) as Axial Restraint for the Perseus over Goodwyn Flowline." UWA research report.

Puech, A., and P. Foray. 2002. "Refined Model for Interpreting Shallow Penetration CPTs in Sands." In *Proceedings of the Annual Offshore Technology Conference*, 2441–49. OnePetro. https://doi.org/10.4043/14275-MS.

Randolph, M. F., and S. Hope. 2004. "Effect of Cone Velocity on Cone Resistance and Excess Pore Pressures." *Proceedings of the International Symposium on Deformation Characteristics of Geomaterials – IS Osaka* 10 (1): 147–152.

Randolph, M. F., R. J. Jewell, K. J. L. Stone, and T. A. Brown. 1991. "Establishing a New Centrifuge Facility." In *International Conference Centrifuge '91*. Balkema, Rotterdam, The Netherlands.

Wroth, H. M., M. F. Bransby, C. D. O'Loughlin, M. F. Silva, M. Cocjin, N. Levy, and H. E. Low. 2022. "Using Near-Surface CPT Data to Predict Foundation Skirt Embedment in Partially Drained Carbonate Sands." In *Cone Penetration Testing 2022 - Proceedings of the 5th International Symposium on Cone Penetration Testing, CPT 2022*, 1149–55. CRC Press/Balkema. https://doi.org/10.1201/9781003308829-175.